

A VENUS-MASS PLANET ORBITING A BROWN DWARF: MISSING LINK BETWEEN PLANETS AND MOONS

A. UDALSKI¹, Y. K. JUNG², C. HAN^{2,*}, A. GOULD³, S. KOZŁOWSKI¹, J. SKOWRON¹, R. POLESKI^{1,3}, I. SOSZYŃSKI¹, P. PIETRUKOWICZ¹, P. MRÓZ¹, M. K. SZYMAŃSKI¹, Ł. WYRZYKOWSKI¹, K. ULACZYK¹, G. PIETRZYŃSKI¹, Y. SHVARTZVALD⁴, D. MAOZ⁴, S. KASPI⁴, B. S. GAUDI³, K.-H. HWANG², J.-Y. CHOI², I.-G. SHIN², H. PARK², V. BOZZA^{5,6}

¹Warsaw University Observatory, Al. Ujazdowskie 4, 00-478 Warszawa, Poland

²Department of Physics, Chungbuk National University, Cheongju 371-763, Republic of Korea

³Department of Astronomy, Ohio State University, 140 W. 18th Ave., Columbus, OH 43210, USA

⁴School of Physics and Astronomy, Tel-Aviv University, Tel-Aviv 69978, Israel

⁵Dipartimento di Fisica "E.R. Caianiello", Università di Salerno, Via Giovanni Paolo II 132, 84084, Fisciano (SA), Italy

⁶Istituto Nazionale di Fisica Nucleare, Sezione di Napoli, Via Cinthia 9, 80126 Napoli, Italy and

*Corresponding author

Draft version April 2, 2018

ABSTRACT

The co-planarity of solar-system planets led Kant to suggest that they formed from an accretion disk, and the discovery of hundreds of such disks around young stars as well as hundreds of co-planar planetary systems by the *Kepler* satellite demonstrate that this formation mechanism is extremely widespread. Many moons in the solar system, such as the Galilean moons of Jupiter, also formed out of the accretion disks that coalesced into the giant planets. We report here the discovery of an intermediate system OGLE-2013-BLG-0723LB/Bb composed of a Venus-mass planet orbiting a brown dwarf, which may be viewed either as a scaled down version of a planet plus star or as a scaled up version of a moon plus planet orbiting a star. The latter analogy can be further extended since they orbit in the potential of a larger, stellar body. For ice-rock companions formed in the outer parts of accretion disks, like Uranus and Callisto, the scaled masses and separations of the three types of systems are similar, leading us to suggest that formation processes of companions within accretion disks around stars, brown dwarfs, and planets are similar.

Subject headings: planetary systems – brown dwarfs – gravitational lensing: micro

1. INTRODUCTION

Brown dwarfs are intermediate in mass between stars and planets, making them important laboratories for testing theories about both classes of objects, including theories about atmospheres, binarity, and formation mechanism. Brown dwarfs are also potentially a laboratory to test theories of planet formation, but detecting planets that orbit brown dwarfs is challenging. Four super-Jupiter planets orbiting brown dwarfs have been detected to date by three techniques: direct-imaging (Chauvin et al. 2004; Todorov et al. 2010), radial-velocity (Joergens & Müller 2007), and microlensing (Han et al. 2013). In the first three cases, the super-Jupiter planet was within a decade in mass of its host and well separated from it, suggesting that these systems more resemble scaled down binary stars than they do the extreme mass-ratio systems that are likely to emerge from accretion disks. In the fourth case, the separation was substantially closer and the mass ratio somewhat more pronounced so that the planet could have formed through the core-accretion scenario that is thought to be the origin of the solar system's gas giants.

With present technology, substantially lower-mass companions to brown dwarfs, composed primarily of ice and rock, can only be discovered using the gravitational microlensing technique. Microlensing does not rely on light from either the host or planet, but rather infers the existence and properties of these bodies from their deflection and magnification of light from a more distant star that is fortuitously aligned with the system. As such, the low-luminosity of the brown dwarf and almost complete absence of light from its low-mass companion do not interfere in any way with the discovery process.

In this paper, we report the microlensing discovery of an intermediate system OGLE-2013-BLG-0723LB/Bb composed

of a Venus-mass planet orbiting a brown dwarf. The system may be viewed either as a scaled down version of a planet plus star or as a scaled up version of a moon plus planet orbiting a star, suggesting that formation processes of companions within accretion disks around stars, brown dwarfs, and planets may be similar.

2. OBSERVATION

Microlensing event OGLE-2013-BLG-0723 was discovered by the Optical Gravitational Lensing Experiment (OGLE-IV) (Udalski et al. 2015) on May 12, 2013 (HJD \sim 2456424.5) using its 1.3m Warsaw telescope at the Las Campanas Observatory in Chile. At $(\alpha, \delta)_{J2000} = (17^{\text{h}}34^{\text{m}}40^{\text{s}}.51, -27^{\circ}26'53''.2)$ [$(l, b) = (-0^{\circ}.02, 2^{\circ}.83)$], the event lies in one of nine fields toward the Galactic bulge that OGLE observes $\gtrsim 1 \text{ hr}^{-1}$, which is sufficient cadence to discover terrestrial planets. In fact, the discovery was triggered by a short ~ 1 day, $\sim 40\%$ brightening of the lensing event that was still in progress at the time of the announcement (Figure 1, left inset), and which was soon suggested to be of planetary origin. Hence, when the event underwent a second much larger (factor 10) anomalous brightening 49 days later, OGLE immediately recognized that it would be crucial to fully characterize this second anomaly. In particular, since such violent brightening is always caused by the source entering a "caustic" (closed curve of formally infinite magnification – see Figure 2), a caustic exit was inevitable. Because these caustic crossings typically last only an hour or so and can occur at any time during the day, OGLE contacted the Microlensing Follow Up Network (μ FUN) which operates a global network of narrow-angle telescopes capable of near 24-hour monitoring of individually important events. With the aid of real-time

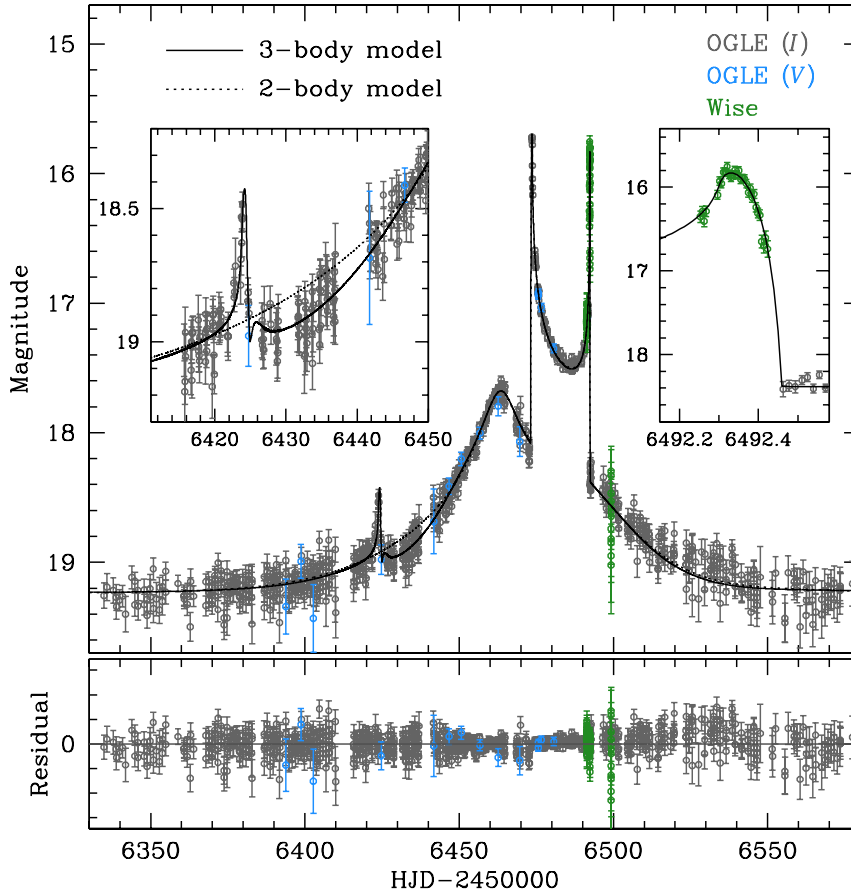


FIG. 1.— Light curve of the microlensing event OGLE-2013-BLG-0723, including models with and without the planet. Left inset shows the planetary anomaly, which includes not just the obvious spike, but also a more extended low level depression. Right inset shows dense coverage of caustic exit, which permitted measurement of the Einstein radius θ_E .

modeling that accurately predicted the time of the exit, the Wise Observatory 0.46m telescope at Mitzpe Ramon, Israel, obtained dense coverage of this exit (Figure 1, right inset).

The principal data were taken in I band. In addition, OGLE obtained some V -band data in order to characterize the microlensed source. Finally, μ FUN obtained H -band observations from the 1.3m SMARTS telescope at Cerro Tololo Interamerican Observatory in Chile. These are not used in the present analysis but will be important for the interpretation of future follow-up observations to cross-check the lens system parameters

The light curve of OGLE-2013-BLG-0723 shows a systematic decline in the baseline. A similar long term linear trend (of opposite sign) was seen in OGLE-2013-BLG-0341 and was eventually traced to a nearby bright star that was gradually moving toward (in that case) the source star, so that more of its flux was being “captured” in the tapered aperture used to estimate the source flux. We searched for such a moving bright star by examining the difference of two images, from 2004 and 2012. We indeed find a dipole from a bright star roughly $1.5''$ away, which is the characteristic signature of such moving stars. Having identified the cause of this trend, we fit for it and remove it.

Photometry of the event was done using a customized pipeline based on the Difference Imaging Analysis method (Alard & Lupton 1998; Woźniak 2000). Because the photometric errors estimated by an automatic pipeline, e_0 , are often

underestimated, the error bars are readjusted by

$$e = k(e_0^2 + e_{\min}^2)^{1/2}, \quad (1)$$

where e_{\min} is a term used to make the cumulative distribution function of χ^2 as a function of lensing magnification becomes linear and the other term k is a scaling factor used to make χ^2 per degree of freedom (dof) becomes unity. The former process is needed in order to ensure that the dispersion of data points is consistent with error bars of the source brightness and the latter process is required to ensure that each data is fairly weighted according to error bars.

3. LIGHT-CURVE ANALYSIS

The principal features of the light curve are a large double-horned profile near the peak, which is a signature of binary microlenses, and a short-lived spike two months earlier, which is characteristic of planetary companions. Modeling these features yields the mass ratios and instantaneous locations of the three bodies relative to the source trajectory. See Figure 2. However, by themselves, these features do not yield either the physical or angular scale of the diagram, nor its orientation on the sky. Rather, the diagram is scaled to the “Einstein radius”, which can be expressed either as an angle θ_E , or as a physical length \tilde{r}_E projected on the observer plane.

The source star and the Earth’s orbit act as “rulers” to determine these two quantities, as well as the angular orientation. The source angular radius θ_* is known from its observed

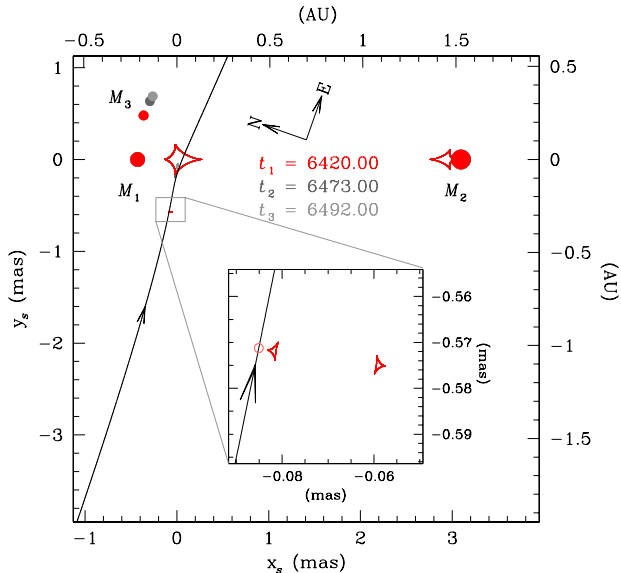


FIG. 2.— Geometry of the lensing event. The curve with an arrow represents the source trajectory. Locations of lens components are marked by filled dots, where M_3 is the planet, M_1 is the planet’s host, and M_2 is the binary companion. The cuspy closed curves are caustics formed by the lens. The inset shows an enlarged view around the caustic that produced the short-term anomaly. The small empty circle on the source trajectory in the inset represents the source size relative to the caustic. We note that the position of the planet and the resulting caustic vary in time due to its orbital motion around its host. Lower/left axes are expressed by angle on the sky in mas, while upper/right axes show projected size of the system in AU. The directions North and East on the sky are indicated

temperature and flux. Hence, when it passes over a caustic (see Figure 2), the finite extent of the source smears out what would be an extremely sharp peak for a point source (Figure 1, right inset). Second, Earth’s accelerated motion induces distortions in the light curve, which fix both \tilde{r}_E relative the size of Earth’s orbit (1 AU) and the orientation of the diagram relative to that of Earth’s orbit, namely the ecliptic. Hence, we are able to display both the angular scale and physical orientation in Figure 2. The mass M and distance D_L of the lens are then given by

$$\frac{1}{D_L} = \frac{\theta_E}{\tilde{r}_E} + \frac{1}{D_S}, \quad \frac{4GM}{c^2} = \tilde{r}_E \theta_E. \quad (2)$$

The first equation follows from simple geometry. Once the distance is known, the second equation follows from Einstein bending angle $\alpha = 4GM/(bc^2)$, where b is the impact parameter of the lens-source approach. See the graphical presentation of the formalism in Gould (2000).

3.1. Microlens Modeling

Full modeling of the light curve ultimately requires a total of 19 parameters, including 14 parameters to describe the lensing system and five flux parameters. Some of these manifest themselves in quite subtle effects. The modeling therefore proceeded in several distinct phases. First, we determine the principal parameters describing the binary-lens system by removing the data for 25 days around the planetary perturbation and fitting the remaining light curve to seven system parameters plus four flux parameters (two for each observatory). These nine include three parameters to describe the underlying point-lens event (t_0, u_0, t_E), three to describe the perturbations induced by the binary companion (s_1, q_1, α), one to

TABLE 1
LENSING PARAMETERS

Quantity	Value
χ^2/dof	4126.8/4073
t_0 (HJD’)	6484.526 ± 0.037
u_0	-0.079 ± 0.002
t_E (days)	68.48 ± 0.01
s_1	5.07 ± 0.02
q_1	3.11 ± 0.02
α (rad)	-1.195 ± 0.003
s_2	0.97 ± 0.02
q_2 (10^{-5})	6.61 ± 0.01
ψ_0 (rad)	-4.936 ± 0.005
ρ (10^{-3})	1.40 ± 0.02
$\pi_{E,N}$	-0.05 ± 0.01
$\pi_{E,E}$	1.35 ± 0.02
ds_2/dt (yr^{-1})	0.81 ± 0.02
$d\psi/dt$ (yr^{-1})	-0.50 ± 0.02
I_S	19.825 ± 0.006
I_B	20.181 ± 0.008

NOTE. — I_S and I_B represent the baseline magnitudes of the source and blend, respectively.

describe the ratio of the source radius to the Einstein radius, $\rho = \theta_*/\theta_E$, and the two-dimensional microlens parallax vector $\boldsymbol{\pi}_E = (\pi_{E,N}, \pi_{E,E})$.

Here t_0 is the time of closest approach to a reference point in the geometry, which is chosen as the “center of magnification” of the caustic traversed by the source, u_0 is the impact parameter in units of θ_E , and t_E is the time required for the source to cross θ_E . We choose θ_E as the Einstein radius of the mass associated with the caustic, which is the total mass for the close-binary case, and the mass of the binary component located closer to the source trajectory for the wide-binary case. This convention leads to similar t_E for the two cases, e.g. (Gould et al. 2014).

The three binary parameters are the separation of the components in units of θ_E , the ratio of the companion to primary component masses, and the angle of the source trajectory relative to the binary axis at t_0 (since parallax causes this to change with time).

The amplitude of the parallax vector is $\pi_E = \text{AU}/\tilde{r}_E$, while its direction is that of the lens-source relative proper motion (in the geocentric frame). In contrast to the lens-source trigonometric relative parallax $\pi_{\text{rel}} = \pi_E \theta_E$, which is a scalar quantity, the microlens parallax requires two parameters because the lens is not directly observed, so the orientation of the lens-source separation relative to the ecliptic is not known a priori. See Gould & Horne (2013). Normally, one would not include parallax in the initial fit, but in this case it is so large that the projected Einstein radius is substantially smaller than Earth’s orbit, $\tilde{r}_E \sim 0.35 \text{ AU}$, so that there is no even approximately good solution without including π_E in the fit.

With this parameterization, we find an excellent fit for the wide-binary case ($s > 1$) but only a crude approximation to the observed light curve for $s < 1$. We then incorporate two-parameter orbital motion, essentially the instantaneous relative transverse velocity of the components in Einstein-radius units. This refinement results in negligible improvement for the $s > 1$ solution, but dramatic improvement in the $s < 1$ solution, so that the two models provide qualitatively similar approximations of the data. However, it is found that the $s < 1$ case is unlikely due to various reasons as discussed in Appendix.

We then restore the data from the planetary perturbation and

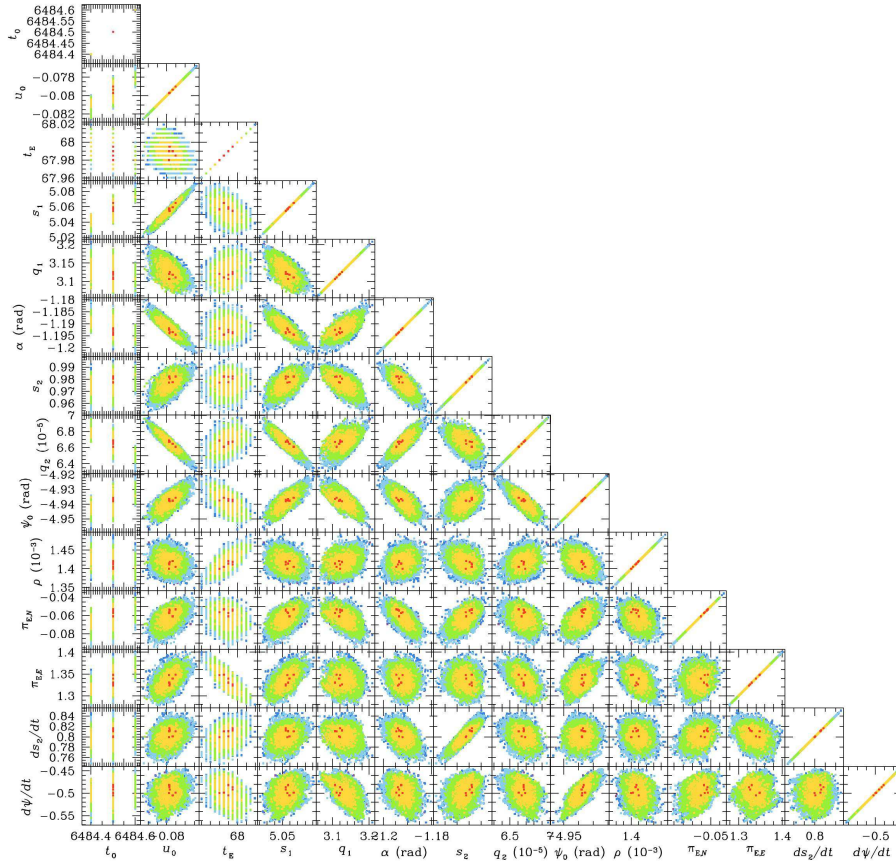


FIG. 3.— Distribution of the microlensing parameters of the best-fit solution, whose central values and errors are shown in Table S1. Color coding indicates points on the Markov Chain within 1 (red), 2 (yellow), 3 (green), 4 (cyan), 5 (blue) σ of the best fit.

add five additional parameters to the fit: $(s_2, q_2, \psi_0, \gamma)$, where $\gamma = (ds_2/dt/s_2, d\psi/dt)$. Here (s_2, q_2) are the separation and mass ratio of the planet relative to its host (the smaller component of the binary), ψ_0 is the angle between binary axis and the planet-host axis at t_0 , and γ is the two dimensional projected velocity of the planet relative to its host. Table 1 shows the best fit parameters. In Figure 3, we also present the distribution of $\Delta\chi^2$ in the parameter space in order to show the uncertainties and correlations between the parameters.

3.2. Origin of Parallax and Orbital Signals

The microlensing parallax signal is quite strong ($\Delta\chi^2 > 1100$), but since the amplitude $\pi_E = 2.7$ is one of the largest ever detected and hence quite unusual. Therefore, it is prudent to check whether this signal is coming mainly from one part of the light curve, which would be suspicious, or from the entire magnified portion of the light curve, as one would expect.

Figure 4 shows that in fact the signal is coming from the whole magnified light curve. It also shows that planetary orbital signal, while much weaker ($\Delta\chi^2 = 41$), is also broadly based. As expected, the orbital signal is more compact than the parallax signal.

3.3. Degeneracy

Because the light curve is well covered, the parameters are well determined. However, the solution is still subject to three well known discrete degeneracies. First, there is a degeneracy between pairs of companion mass ratio and normalized separation (q, s) , with one lying inside the Einstein radius ($s < 1$)

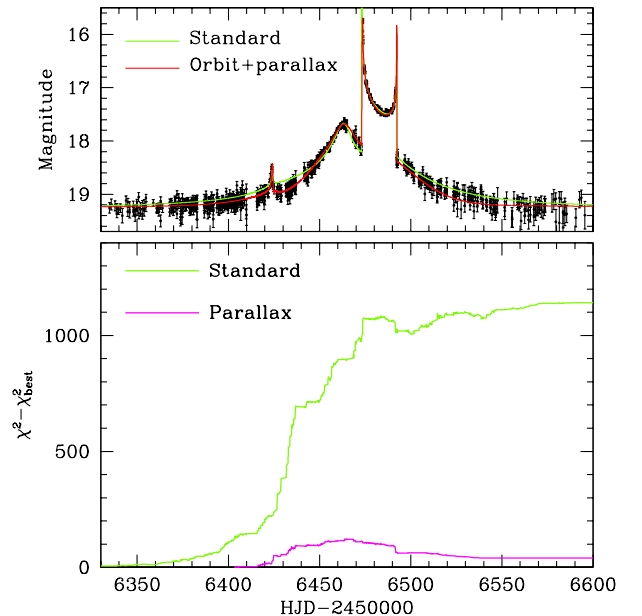


FIG. 4.— Cumulative distributions of $\Delta\chi^2$ from the best-fit (orbit+parallax) model for the standard (green curve) and parallax (magenta curve) models.

and the other outside. This degeneracy is fully understood at first (Griest & Safizadeh 1998; Dominik 1999) and second (An 2005) order for the case that the binary is approximated as static. We find that within this context there is no “close”

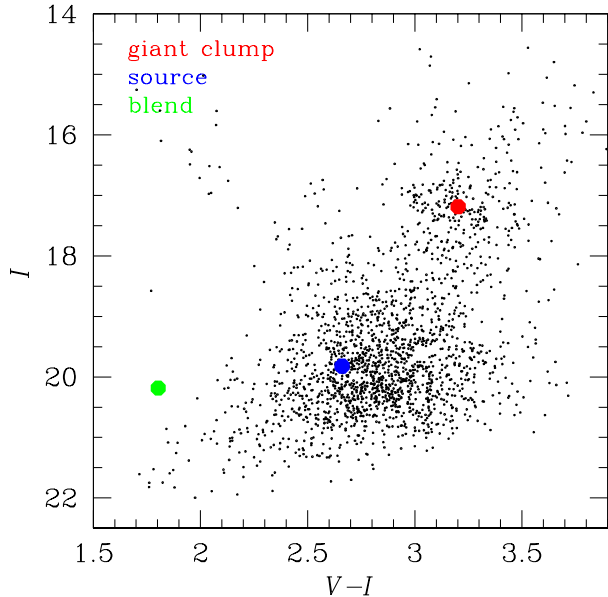


FIG. 5.— Location of the source star in the color-magnitude of stars in the nearby field. Also marked are the positions of the centroid of the red clump giant stars and of the blend. For the first two, the error bars are smaller than the points. For the last, the magnitude is secure but the error in the color (not shown) is both large and uncertain, being at least 0.2 mag.

solution, i.e., $\Delta\chi \sim 2000$ between close and wide solutions. However, if both close and wide binary models are permitted two degrees of orbital motion, i.e. ds_2/dt and $d\psi/dt$, then the wide solution shows essentially no improvement while the close solution improves dramatically and matches the wide solution. In Appendix, we discuss the mathematical and physical nature of this new variant of the close/wide degeneracy and show that it implies that the wide solution is strongly favored. We also present additional corroborating arguments that this is the case. We therefore consider only the wide solution.

Second, if the source lay on the ecliptic, the entire solution could be “flipped” relative to the ecliptic without changing the light curve. Since the source lies just 4° from the ecliptic, this degeneracy is close to exact, with the preferred solution favored by only $\Delta\chi^2 = 38$. While this is enough to clearly favor one solution, the main point is that the two solutions yield almost identical physical implications.

Finally, Figure 2 shows the small planetary caustics just to the right of the source trajectory. In principle, there could be another solution with these caustics just to the left. However, this geometry is unable to reproduce the long slow “depression” that follows the planetary anomaly and is due to a demagnification “valley” that follows the axis defined by the two small caustics. Hence, the solution is both unique and measured with good precision.

3.4. Characteristics of the Source Star and Blended Light

We determine the angular source radius θ_* based on its dereddened color $(V-I)_0$ and brightness I_0 (Yoo et al. 2004), which we determine from their offsets from the centroid of the red giant clump $[(V-I), I]_{0,\text{clump}} = (1.06, 14.45)$ (Bensby et al. 2011; Nataf et al. 2013), under the assumption that the source and the clump giants suffer similar extinction. Figure 5 gives a graphic representation of this procedure, and also shows the position of the star (or ensemble of stars) that are blended

with the source. That is, in each band, the light-curve flux is modeled as $F(t) = f_s A(t) + f_b$, where A is the magnification. The source and blend magnitudes are then derived from the fit parameters f_s and f_b , respectively.

We find $(V-I, I)_0 = (0.52, 17.09)$. From this color and flux, we derive $\theta_* = 0.98 \pm 0.08 \mu\text{as}$ by converting $(V-I) \rightarrow (V-K)$ (Bessell & Brett 1988) and then applying a color/surface brightness relation (Kervella et al. 2004). The derived color is well bluerward of the overwhelming majority of Galactic bulge stars, except for horizontal branch stars, which are substantially brighter. Hence, the source is almost certainly in the Galactic disk. Disk sources are rare in general (a few percent) partly because the source must be farther than the lens with the lenses being mostly in the bulge or fairly far in the disk, and partly because the column density of bulge stars is higher than for disk stars. However, given that this particular lens lies far in the foreground ($D_L \sim 0.5$ kpc), it is not unexpected for the source to lie in the disk.

Based on the source color and magnitude, we estimate its distance $D_S = (7 \pm 1)$ kpc. The exact distance plays no role in the determination of θ_* because this depends only on the flux $F \propto L/D_S^2$, not the luminosity L and distance separately, provided that the source lies behind essentially all the dust. Given that the source sits 360 pc above the Galactic plane, this is almost certainly the case. The uncertainty in the source distance also enters into the uncertainty in the lens distance through Equation (2). In practice, however, this leads to an error in source distance of only 4%, which is small compared to other sources of errors.

Finally, we note that the source color indicates a temperature $T \sim 6100\text{K}$, which leads to an estimate of the limb-darkening coefficient (needed for modeling the caustic exit) of $u = 0.495$ (Claret 2000).

In most microlensing events, the blended light f_b is just a nuisance parameter, but in the present case it is potentially very important. We first note that while the I -band magnitude is secure, the error in the $(V-I)$ color (not shown) is quite large. First, the formal error of the fit is 0.2 mag. In addition, in contrast to the source flux, which is determined solely from changes in brightness, the blend flux depends on the accuracy of the baseline photometry. This can be corrupted by bright nearby blends, which are plainly visible on the images, and by stars that are too faint to be identified. Hence, we consider the color to be only indicative and do not make use of it in further discussion. However, the I band measurement is too bright to be the OGLE-2013-BLG-0723LA by about 1.5 mag.

To further understand the origin of this light, we measure the position of the source relative to the “baseline object”, which is an unresolved blend of the source with the star or stars giving rise to f_b . We find $\Delta\theta_{\text{base}} = 55$ mas. Since the blend contains 43% of the baseline light, this implies that it is naively offset from the source by $\Delta\theta_{\text{blend}} = \Delta\theta_{\text{base}}/0.43 = 125$ mas. However, while the source position can be measured extremely well because it becomes highly magnified, the “baseline object” is subject to contamination from unseen stars as well as the wings of nearby bright stars. We conclude that the centroid of blend light is separated from the source by $\Delta\theta_{\text{blend}} \lesssim 125$ mas. Because the surface density of stars $I < 20.1$ in this field is $\lesssim 0.1 \text{ arcsec}^{-2}$ (Holtzman et al. 1998), the probability that this blended light lies so close to the source (and lens) by chance is $< 1\%$. It is therefore most likely a companion to either the source or lens. This issue can be resolved by obtaining AO images at two epochs to deter-

TABLE 2
PHYSICAL PARAMETERS

Quantity	Value
Mass of the planet	$0.69 \pm 0.06 M_{\oplus}$
Mass of the host	$0.031 \pm 0.003 M_{\odot}$
Mass of the binary companion	$0.097 \pm 0.009 M_{\odot}$
Distance to the lens	0.49 ± 0.04 kpc
Projected planet-host separation	0.34 ± 0.03 AU
Projected separation between binary components	1.74 ± 0.15 AU
Relative lens-source proper motion (geocentric)	3.75 ± 0.33 mas/yr
Relative lens-source proper motion (heliocentric)	14.5 ± 1.3 mas/yr

mine whether its proper motion is consistent with the source or lens. If it proves to be associated with the lens, then this is a four-body system consisting of a brown dwarf orbited by a Venus-mass planet, with both orbiting a very low-mass star, and with this entire group orbiting another star that is roughly double the mass of the star that contributed to the microlensing event.

3.5. Physical Parameters

The principal physical parameters are given in Table 2. From the determined masses of the individual lens components, it is found that the lens is a triple system that is composed of a Venus-mass planet ($0.69 M_{\oplus}$) orbiting a brown-dwarf host ($0.031 M_{\odot}$) that is accompanied by a low-mass star ($0.097 M_{\odot}$). The projected planet-host separation is 0.34 AU, while the separation between the binary components is 1.7 AU. The system is located at a distance 490 pc toward the Galactic center.

Note that we give the proper motion in both the geocentric frame in which the measurements were actually made, and the heliocentric frame, which will be useful for comparison with future observations. Since D_L is known, the conversion from geocentric to heliocentric frames is straightforward.

3.6. Which Binary Component is Host to the Planet?

From Figure 2 or Table 1, the planet’s projected position is $5.07/0.97 = 5.2$ times closer than the stellar companion. If the planet were orbiting the more massive companion, this would occur with probability $< 4\%$. In addition, in order to ensure stability of the 3-body system, the brown dwarf would have to be behind (or in front of) the star-planet system by a at least factor of 3 larger distance than the projected separation of the brown dwarf and star. This chance alignment further reduces the probability by a factor 3^2 . Hence, while this configuration is possible in principle, it has extremely low probability. A very similar argument applies to a circumbinary configuration, in which the planet’s orbit is at least three times larger than the separation between the brown dwarf and star, but just happens to be seen in projection close to the brown dwarf.

4. DISCUSSION

OGLE-2013-BLG-0723LBb is a missing link between planets and moons. That is, its host OGLE-2013-BLG-0723LB, being a brown dwarf in orbit around a self-luminous star, is intermediate between stars and planets, in both size and hierarchical position. Moreover, the scaled mass and host-companion separation of OGLE-2013-BLG-0723LB/Bb are very similar to both planets and moons in the solar system. See Table 3. Both Uranus and Callisto are believed to have formed in the cold outer regions of their respective accretion disks, and are mostly composed of the raw materials of such

regions: ice with some rock. In the case of Uranus, it is believed to have been formed closer to the current location of Saturn (10 AU) and to have migrated outward. In the table, the companion-host separations are scaled to the host mass. This is appropriate because the “snow line”, the inner radius at which icy solids can form (2.7 AU in the solar system) increases with host mass, probably roughly linearly. A plausible inference from the first three lines of Table 2 is that these processes scale all the way from solar-type stars hosting planets, to brown dwarfs hosting “moon/planets”, to giant planets hosting moons.

However, while OGLE-2013-BLG-0723LBb is almost certainly orbiting OGLE-2013-BLG-0723LB today, we cannot guarantee that it was born there. Planets in relatively close binaries (like OGLE-2013-BLG-0723LA,B) can jump from one star (or in this case, brown dwarf) to the other, if the system is dynamically perturbed (Kratter & Perets 2012). If this is what happened to OGLE-2013-BLG-0723LBb, then would have been captured from an orbit around OGLE-2013-BLG-0723LA to its current orbit around OGLE-2013-BLG-0723LB. It would then be similar to Triton, which was captured by Neptune out of solar orbit. Table 3 shows that the Neptune-Triton system in its current configuration is also not terribly different than a scaled version of OGLE-2013-BLG-0723LB/Bb.

It will be interesting to model the dynamics of the triple system OGLE-2013-BLG-0723LA,B,b, but it would be premature to do so. This is because there is likely a fourth member of this system that is more massive and luminous than the other three, and which is separated by of order 100 AU or less. If confirmed, this member could significantly impact the system dynamics via the Lidov-Kozai mechanism. The principal evidence for this fourth member is that there is excess light in the aperture that is too bright to be the primary star OGLE-2013-BLG-0723LA, and is so closely aligned with the source that it is unlikely to be a random interloper. Because the source flux is known from the H -band light curve (which is not included in the present analysis), it will be straightforward to subtract out the source light from a high-resolution adaptive optics (AO) image and determine the exact location of the blended light. If well separated, then its association with the lens can be established from its proper motion, derived from observations at two epochs, which can be compared with Table 2. If directly superposed in the AO images, then it is almost certainly associated with either the source or the lens because of the extremely low probability of a random interloper. The two possibilities can be distinguished based on the apparent color because the source is highly reddened by dust, but the lens sits in front of the great majority of the dust.

OGLE-2013-BLG-0723LBb is the second terrestrial mass planet orbiting one member of a binary system composed of two very low mass objects. The other was OGLE-2013-BLG-0341LBb. Gould et al. (Gould et al. 2014) showed that if all low-mass stars were in such systems, roughly one should have been detected. They noted that no strong statistical inference could be derived from this fact because, for example, if only 1% of low-mass stars were in such systems, there would be a 1% chance to find one. Because the question about the frequency of these systems was being framed a posteriori, a 1% effect is not particularly significant.

However, OGLE-2013-BLG-0723LBb reproduces three of the four elements that went into their estimate of the frequency of such detections, namely small probability of pass-

TABLE 3
COMPANION/HOST PAIRS

Host/Companion	$M_{\text{comp}}/M_{\text{host}}$ (10^{-5})	$r_{\text{c-h}}/M_{\text{host}}$ (AU/ M_{\odot})
Uranus/Sun	4.4	19
OGLE-2013-BLG-0723LBb/B	6.6	11
Callisto/Jupiter	5.7	13
Triton/Neptune	21	46

ing by the planetary caustic, small probability of crossing the central (binary) caustic, and location in a high-cadence OGLE fields. The fourth criterion, source magnitude brighter than $I_S = 18.5$, is not satisfied, since $I_S \sim 19.8$. If the limit were extended to $I_S < 20$, the total number of available events would roughly double. Hence, the prediction would rise to two. With

two predicted and two detected, the probability that these are extremely rare drops roughly as the square, i.e., roughly 10^{-4} probability of this occurring by chance if only 1% of these stars were in such systems. Hence, while there is still no compelling evidence that these systems are extremely common, at least they are not extremely rare. Further, the current detections remain consistent with the hypothesis that these systems are ubiquitous.

The OGLE project has received funding from the National Science Centre, Poland, grant MAESTRO 2014/14/A/ST9/00121 to AU. Work by C.H. was supported by Creative Research Initiative Program (2009-0081561) of National Research Foundation of Korea. A.G. and B.S.G. acknowledge support from NSF AST-1103471. B.S.G., A.G., and R.W.P. acknowledge support from NASA grant NNX12AB99G.

APPENDIX

RESOLUTION OF THE CLOSE/WIDE DEGENERACY

In the main text of the paper, we stated that the wide solution was consistent with a static binary while the close solution required substantial orbital motion to match the wide-solution light curve. At first sight this seems qualitatively reasonable since close binaries have shorter periods than wide ones. However, only one of these solutions corresponds to the physical system, while the other is merely a mathematical reflection of it. Hence, the real question is not whether each solution is physically plausible but what is the relative likelihood where each solution, if it were real, could generate the other as a doppelganger.

Before addressing this, some comments must be in order as why this degeneracy is appearing in this case and how likely it will be to appear generically. In the simplest cases two solutions appear because to first order, the quadrupole expansion of the close-binary potential and the tidal expansion of the wide-binary potential are identical and so (to this order) produce identical caustics (Griest & Safiedah 1998; Dominik 1999). Contemporaneously, it was noticed that in more typical cases, the degeneracy could remain extremely severe even though the caustics were not actually identical and, indeed, appeared rotated relative to each other (Fig. 8 of (Afonso et al. 2000)). This was ultimately explained by carrying out the analysis to second order (An 2005). That is, an additional degree of freedom (basically, rotation) could compensate for the slower convergence of the potential. For wide binaries, the potential converges more slowly as the mass ratio of the companion increases and as its separation gets closer. This is well illustrated by small mass-ratio, e.g., planet/star, systems. Topologically, the two caustics are the same, but geometrically they are very different. The planet has a relatively weak effect on the stellar potential, meaning that the star’s caustic (“central caustic”) is well-described by low-order terms and hence subject to the close/wide degeneracy. By contrast, the planetary caustic is strongly perturbed and not subject to this degeneracy (unless the separation is very large).

In the present case, the caustic feature in the light curve of the wide solution is associated with the lower-mass companion, and the mass ratio is relatively large. Hence, one expects that (as in the planetary case) higher order terms will play a relatively large role. And indeed they prove to be too large to permit the degeneracy analyzed by (An 2005). Orbital motion then provides the additional degree of freedom to compensate for the non-trivial higher-order terms.

Consider then a wide binary that is qualitatively similar to the present case. Regardless of details, its light curve can always be mimicked by including the appropriate amount of orbital motion. On the other hand, consider a (real) close binary with the (s, q) parameters predicted by the wide binary but with so far unspecified orbital parameters. Can this system “generate” a static wide binary with the same light curve? The answer is: only if its orbital parameters happen to lie in a narrow range around those predicted by the wide pair. Otherwise, the static wide binary would have been consistent with a wide range of close-binary orbital motions. Because $\Delta\chi^2$ is quite large, the fine-tuning requirements of the close solution are severe. This is the principal reason that we discount it.

However, in addition, if the close solution is spurious and merely tuned to the mathematical requirements of matching the wide solution, it is likely to have characteristics that are atypical of real systems, which can be a further indication of its spurious nature. We note two such features. First, the ratio of projected kinetic to potential energy (Dong et al. 2009) is quite low

$$\beta \equiv \left(\frac{E_{\text{kin}}}{E_{\text{pot}}} \right)_{\perp} = \frac{(s\theta_E D_L / \text{AU})^3 (\gamma \text{ yr})^2}{M/M_{\odot}} = 0.023 \quad (\text{A1})$$

compared to typical values $0.1 \lesssim \beta \lesssim 0.5$. The three physical effects that can produce low β are 1) it is near apocenter of an extremely eccentric orbit, 2) our line of sight happens to be almost tangent to the orbital velocity vector, or 3) we happen to view the system edge on, so that its semi-major axis is much larger than its projected separation. Since the unprojected ratio typically has values $E_{\text{kin}}/E_{\text{pot}} \sim 0.5$ reducing this number by a factor ~ 20 via projection effects requires some fine tuning. However, in the present case there is an additional complication: the third option generates the need for an additional low probability event. That is, if the two stars are extended along the line of sight, then either this projection must be very great to allow the planet to have a stable orbit around one star (actually brown dwarf), to the planet itself must be seen in projection next to the pair despite

the fact that its orbit is at least three times that of the extended binary. Finally, we note that the source star is four times fainter in the close model. Since its color (so spectral type) is still the same, this places it twice as far as in the wide solution, where the density of such stars is about a factor 40 smaller. This is somewhat compensated by the eight times larger phase space, but still does further reduce the probability of this solution by a factor 5.

All the arguments given above make the close-binary solution very unlikely but they do not exclude it. However, this solution can also be tested by direct imaging. Since there are compelling reasons to conduct such imaging, possibly at several epochs, no special effort is required to do this. If these observations reveal a blend that is substantially brighter than the source, then the close solution will be confirmed. The expected baseline magnitudes of the source and blend are $(I_S, I_B) = (21.28, 19.42)$, respectively. If the wide solution is correct, we expect the blend and source to be comparable (depending on their $I-H$ colors).

REFERENCES

- Afonso, C., et al. 2000, ApJ, 532, 340
 Alard, C. & Lupton, R. H. 1988, ApJ, 503, 325
 An, J. H. 2005, MNRAS, 356, 409
 Bensby, T., et al., 2011, A&A, 533, 134
 Bessell, M. S. & Brett, J. M. 1988, PASP, 100, 1134
 Chauvin, G., et al. 2004, A&A, 425, L2
 Claret, A. 2000, A&A, 363, 1081
 Dominik, M. 1999, A&A, 349, 108
 Dong, S., et al. 2009, ApJ, 695, 442
 Gould, A. 2000, ApJ, 542, 785
 Gould, A., et al., 2014, Science, 345, 46
 Gould, A., & Horne, K. 2013, ApJ, 779, 28
 Griest, K., & Safizadah, N. 1998, ApJ, 500, 37
 Han, C., et al., ApJ, 2013, 778, 38
 Holtzman, J. A., et al. 1998, AJ, 115, 1946
 Joergens, V., & Müller, A. 2007, ApJ, 666, L113
 Kervella, P., et al. 2004, A&A, 426, 297
 Kratter, K. M. & Perets, H. B. 2012, ApJ, 753, 91
 Nataf, D. H., et al., 2013, ApJ, 769, 88
 Todorov, K., et al. 2010, ApJ, 714, L84
 Udalski, A., Szymański, M.K. & Szymański, G. 2015, Acta Astron., 65, 1
 Woźniak, P. R. 2000, Acta Astron., 50, 421
 Yoo, J., et al., 2004, ApJ, 603, 139